Correlation effects in the high formal oxidation-state compound Sr_2CoO_4

K.-W. Lee and W. E. Pickett
Department of Physics, University of California, Davis, California 95616, USA
(Received 3 March 2006; published 22 May 2006)

Two recent reports confirm that the newly synthesized Sr_2CoO_4 (formal oxidation state Co^{4+}) shows a high Curie temperature (~250 K), but they report different moments of 1.8 μ_B and 1 μ_B per Co. Using both commonly used functionals in the correlated band approach (LDA+U) as well as the local spin density approximation (LSDA), the combined effects of correlation and hybridization with O $2p$ states are calculated and analyzed. Sr_2CoO_2 is already ferromagnetic within LSDA ($M=1.95$ μ_B). Increasing U from zero, the two LDA+U schemes affect the moment oppositely out to a critical value $U_c=2.5$ eV, at which point they transform discontinuously from different states to the *same* large U state. Fixing U at U_c, fixed spin moment calculations show similar behavior out to a minimum at 1 μ_B (a half metallic state), beyond which the fully localized-limit scheme jumps to a state with energy minimum very near 2 μ_B (very close to the LSDA moment). Although the energy minima occur very near integer values of the moment/Co (1 μ_B,2 μ_B), the strong $3d-2p$ mixing and resulting $3d$ orbital occupations seem to preclude any meaningful $S=\frac{1}{2}$ or $S=1$ assignment to the Co ion.

DOI: 10.1103/PhysRevB.73.174428 PACS number(s): 71.20.Be, 71.27.+a, 71.30.+h, 75.30.Gw

I. INTRODUCTION

First row ($3d$) transition metal ions in high oxidation states have been of interest for some time, due to their competing and delicate spin states. There are still several cases where behavior is not understood, indeed, sometimes (due to sample questions arising from difficulty in synthesis) the data are not unambiguous. The best known, and most thoroughly studied, example is that of the quasi-two-dimensional (2D) cuprates, which when hole-doped become high-temperature superconductors. In their undoped state they are Cu^{2+}-based antiferromagnetic insulators. Hole doping drives the Cu oxidation state toward the unstable (practically nonexistent) Cu^{3+} state. At a doping level of 0.15–0.20 holes/Cu optimal superconductivity is reached. They can be doped beyond that level, when they become conventional metallic Fermi liquids. Upon hole doping the "oxidation state" designation must be interpreted with care, since it is clear that the holes go onto the oxygen ions to a large degree.

Another high-oxidation-state ion is Co^{4+}. This ion has recently gained wide exposure due to the unusual properties of Na_xCoO_2, including the discovery[1] that this system becomes superconducting (4.5 K) around $x=0.3$ when it is hydrated. This value of x suggests that the Co ion is 70% of the way to being Co^{4+}, or alternatively, 70% of the ions are Co^{4+} while 30% are Co^{3+}. This system is however metallic for all x except for Na ion-, orbital-, spin-, and charge-ordering[2] precisely at $x=0.5$ (precisely what is responsible is not yet clear). There is magnetism and correlated electron behavior for $x>0.5$ (the Co^{3+} end) while for $x<0.5$ the materials appear to be weakly correlated nonmagnetic metals. While there has been much expectation that the (metastable) endpoint member CoO_2 (nominally, Co^{4+}, d^5) is a Mott insulator, the evidence is that it remains a nonmagnetic metal.[3] Calculations indicate[4] that, as in the cuprates, upon hole doping from the Co^{3+} end, much of the charge difference occurs on the O ion.

The $La_{2-x}Sr_xCoO_4$ system (LSCoO) with two-dimensional layered K_2NiF_4 structure has become interesting because of its magnetic and electrical properties. In this system the formal oxidation state $Co^{(2+x)+}$ near the La end is not unusually high, so its behavior might be expected to be readily understandable. With increasing Sr concentration x, LSCoO shows a structural transition from orthorhombic to tetragonal (i.e., a lattice constant $b\rightarrow a$) around $x=0.5$, with enhanced two-dimensional electronic properties.[5] The structural transition may be connected to an antiferromagnetic-ferromagnetic transition (the maximum Curie temperature $T_C=220$ K at $x=0.9$),[6] accompanying a magnetic change that has been interpreted in terms of a Co^{3+} spin-state transition from high spin to intermediate spin configurations around $x=0.7$.[7] There is another suggestion that at $x=1$ the system is a high-spin, low-spin charge-ordered state.[8] However, there is no agreement among the measurements on the magnetic behavior[6,9–11] nor metallic behavior.[6,12] The end member $x=0$ is an antiferromagnetic (AFM) insulator with Néel temperature $T_N=275$ K.[13]

Although earlier studies were confined to the range below $x=1.4$, recently the end member Sr_2CoO_4, formally Co^{4+}, was synthesized by Matsuno *et al.*[14,15] and by Wang and Takayama-Muromachi[16] and Wang *et al.*,[17] and characterized as FM with high Curie temperature $T_C\approx 250$ K. However, their differing synthetic methods have led to different properties. Matsuno *et al.*[14,15] synthesized a single-crystalline thin film using pulsed-laser deposition, while Wang and Takayama-Muromachi[16] and Wang *et al.*[17] produced polycrystalline samples under high-pressure, high-temperature conditions. The former shows metallic T-dependent resistivity below T_C, although it has definitely higher resistivity of order of $10^{-4}-10^{-3}$ Ω cm at low T than in a typical metal. The pressure-synthesized samples show nearly temperature independent resistivity (perhaps due to polycrystallinity), but with similar magnitude. The more confusing difference is in the observed saturation magnetic moment, 1.8 μ_B/Co and 1 μ_B/Co, respectively. Nevertheless, the sample with the

smaller ordered moment has been observed[16] effective (Curie-Weiss) moment $p_{\text{eff}}=3.72\ \mu_B$, characteristic of a much higher $S=3/2$ spin configuration. Such a moment would suggest a much higher-ordered moment, $\langle S_x\rangle \sim 3\ \mu_B$.

The related perovskite system $La_{1-x}Sr_xCoO_3$ [formally $Co^{(3+x)+}$] has been studied for some time.[18–24] Its magnetic properties are also altered by Sr concentration x: nonmagnetic for $x<0.05$, spin glass for $0.05\leqslant x<0.2$, and ferromagnetic above $x=0.2$. For the end member, $SrCoO_3$ ("Co^{4+}") shows metallic conductivity and has magnetic moments 1.25 and 0.1 μ_B for Co and O, respectively,[18] whereas the ground state of $LaCoO_3$ is a nonmagnetic band insulator. Excitations of $LaCoO_3$ have been interpreted in terms of a locally orbitally ordered excited state.[24,25]

In this paper, we look in some detail at the electronic and magnetic structure of Sr_2CoO_4 both as uncorrelated, using the local spin density approximation (LSDA), and viewing effects of correlation as described by the LDA +Hubbard U (LDA+U) method. Both commonly used LDA+U functionals are employed, and their results are compared and contrasted. A number of unusually rich magnetic phenomena arise (including a half metallic phase), reflecting the strong hybridization with O $2p$ states that complicates the accommodation of correlation effects on the Co ion.

II. STRUCTURE AND CALCULATION

Sr_2CoO_4 has the bct K_2NiF_4-type structure, space group $I4/mmm$ (No. 139), pictured in Fig. 1. The Co-planar O (PO) bond length (1.878 Å) is shorter by about 6% than that of Co-apical O (AO) (1.988 Å). The distorted CoO_6 octahedron, elongated along c axis, leads to crystal field splitting of $t_{2g}\rightarrow \mathrm{E}_g(d_{xz},d_{yz})+\mathrm{B}_{2g}(d_{xy})$ and $e_g\rightarrow \mathrm{A}_g(d_{3z^2-r^2})+\mathrm{B}_{1g}(d_{x^2-y^2})$ states. We have used the lattice constants $a=3.755$ Å, $c=12.6$ Å, and apical O (0.1578) and Sr (0.3544) internal parameters optimized by Matsuno *et al.*,[14] which are consistent with the experimentally measured values by Wang and Takayama-Muromachi.[16]

Our calculations were carried out within the LSDA and LDA+U approaches with the full-potential nonorthogonal local-orbital (FPLO) method.[26] Both commonly used schemes of the LDA+U method were employed so comparisons of the predictions could be made. Both forms have the same Hubbard-like density-density interaction

$$E_U=\frac{1}{2}\sum_{m\sigma\neq m'\sigma'}[U_{mm'}-\delta_{\sigma,\sigma'}J_{mm'}]n_{m\sigma}n_{m'\sigma'}, \qquad (1)$$

where $\{n_{m\sigma}\}$ is a site occupation set and J is intraexchange integral. The form displayed here is schematic in the sense that it does not display all of the indices involved in the full coordinate-system-independent form that is implemented in the code. The two LDA+U approaches differ only in the method of treatment of the "double-counting" term, intended to subtract out the shell-averaged interaction that has already been included in LSDA. One choice is the so-called around mean field (AMF) scheme, which is expected to be more suitable when the on-site Coulomb repulsion U is not so strong.[27] The other choice, called the fully localized limit (FLL) (also called "atomic limit"), is more appropriate for large U systems.[28] The methods to treat the double counting problem in the both schemes are given by

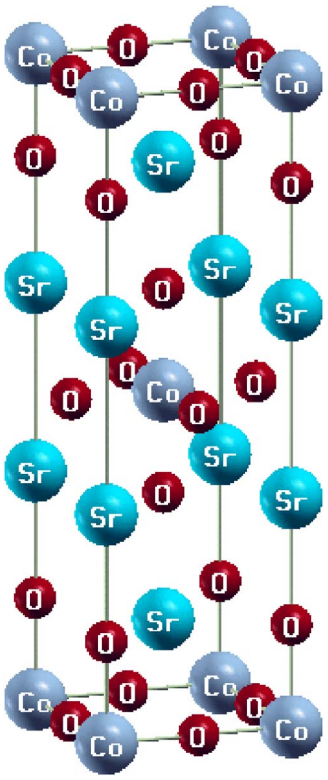

FIG. 1. (Color online) Crystal structure of Sr_2CoO_4, a body-centered-tetragonal type. The planar O-Co bond length is 1.878 Å, about 6% shorter than the apical O-Co bond length. Lattice constants used here are $a=3.755$ Å and $c=12.6$ Å.

$$E^{dc}_{\text{AMF}}=\frac{1}{2}\sum_{m\sigma\neq m'\sigma'}[U_{mm'}-\delta_{\sigma,\sigma'}J_{mm'}]\bar{n}\bar{n},$$

$$E^{dc}_{\text{FLL}}=\frac{1}{2}\sum_{m\sigma\neq m'\sigma'}[U_{mm'}-\delta_{\sigma,\sigma'}J_{mm'}]\bar{n}_\sigma\bar{n}_{\sigma'}, \qquad (2)$$

where $\bar{n}$ is the shell-averaged occupation, while $\bar{n}_\sigma$ is its spin-decomposed analog. These double-counting terms can be written in other forms that emphasize other aspects of the interaction.[29] However, this form is illustrative because it emphasizes that the difference lies in the magnitude of the (self-consistent) atomic moment. Clearly it is only the spherically averaged values of U and J that enter the double-counting terms. The difference between the two forms is that the double-counting term, and the resulting potential, includes a spin dependence in the FLL form.

The fully relativistic scheme of FPLO (Ref. 30) was used when spin-orbit coupling (SOC) in LSDA was necessary. The choice of basis orbitals were Sr $(4s4p)5s5p4d$, Co $(3s3p)4s4p3d$, and O $2s2p(3s3p3d)$. (The orbitals in parentheses indicate semicore or polarization orbitals.) The Brillouin zone was sampled by a regular mesh containing up to 641 irreducible **k** points for LSDA and LDA+U, and 1639

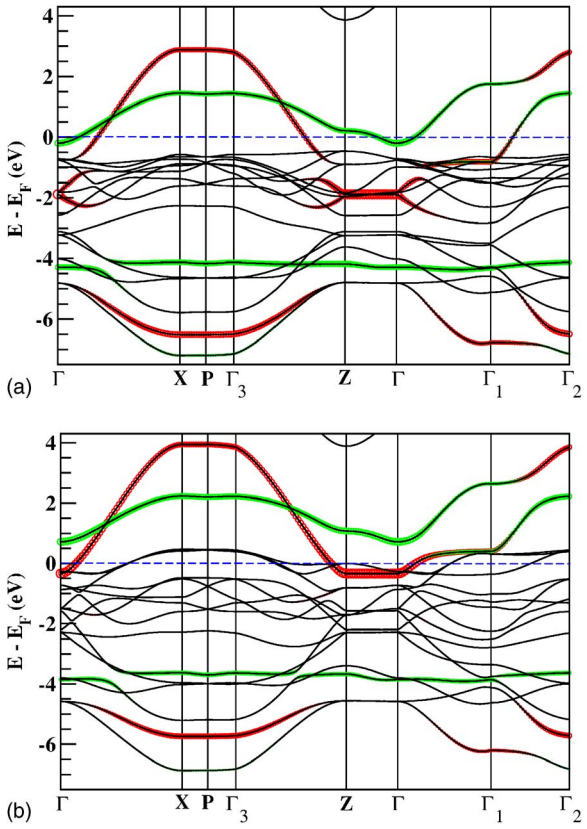

FIG. 2. (Color online) FM LSDA majority (upper) and minority (lower) band structures along symmetry directions. The thickened (and colored) lines emphasize Co $d_{3z^2-r^2}$ (green or light) and $d_{x^2-y^2}$ (red or black) characters, which form bonding and antibonding bands with apical and in-plane O p_σ states, respectively. The symmetry points for the body-centered-tetragonal structure follow the Bradley and Cracknell notation as given in Fig. 5. The dashed horizontal line denotes the Fermi energy.

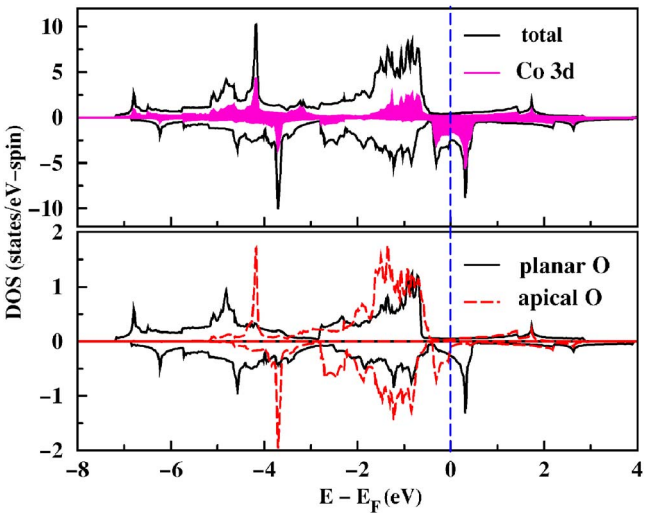

FIG. 3. (Color online) Total and atom-projected densities of states for LSDA FM calculation. Near E_F, there is a van Hove singularity in the minority channel. Although AO is almost fully occupied, the minority of PO is partially occupied, resulting in a large magnetic moment for PO (for details, see text). Additionally, the bandwidth of AO is less than that of PO by 40%. The DOS at E_F $N(0)$ is 2.90 states/electron volt per both spins.

irreducible **k** points for SOC and fixed spin moment (FSM)[31] calculations that require more careful treatment near the Fermi level (E_F).

III. UNCORRELATED TREATMENT

A. Electronic structure

The FM LSDA band structures, exhibiting total magnetic moment $M=1.95$ μ_B that is only accidentally near an integer value, are shown in Fig. 2. The five Co $3d$ bands and three $2p$ bands of each O constitute an entanglement of 17 hybridized bands for each spin, with total $p-d$ bandwidths of 10 and 11 eV for the majority and minority bands, respectively. The strong hybridization throughout the bands is evident in the corresponding total DOS and accompanying atom-projected DOS, shown in Fig. 3. The orbital-projected densities of states, given in Fig. 4, shows that the crystal field splitting of 2 eV, identified from the density of states, between t_{2g} and e_g manifolds is only a little higher than the exchange splitting 1.3 eV. As noted earlier, these t_{2g} and e_g designations are broken down by the $4/m$ symmetry of the Co site. The electronic structure shows clear quasi-two-dimensionality, consistent with resistivity measurement by Matsuno *et al.*[14,15]

In Fig. 2, the $pd\sigma$ and $pd\sigma^*$ bands (for each of $d_{x^2-y^2}$ and $d_{3z^2-r^2}$ orbitals) are highlighted. The more dispersive bands (darker, or red) arise from bonding and antibonding interactions between Co $d_{x^2-y^2}$ and PO p_σ states. The bonding and antibonding bands have a separation of 10 eV at the X point, this total width arising from a combination of the differences between the t_{2g} and $2p$ site energies, and the hybridization between them. The dispersion of the antibonding (upper) band can be described roughly by effective hopping amplitude $t=0.40$ eV (majority) and $t=0.53$ eV (minority). The behavior of the $d_{x^2-y^2}$ band is similar to that observed in the high T_c superconductor La_2CuO_4, in which this antibonding band plays a central role,[32,33] but it is mostly unoccupied here. However, with the lower number of $3d$ electrons the cobaltate electronic structure is influenced more strongly by the t_{2g} manifold, which forms relatively flat bands, the top of which hovers around the Fermi energy. In the minority bands, a van Hove singularity lies at E_F at the Z point, perhaps contributing to the positioning of the Fermi level and hence to the total moment.

The less dispersive highlighted bands (green, or lighter), lying in the 0–2 eV range, arise from the antibonding interaction of Co $d_{3z^2-r^2}$ and AO p_σ states. The bonding band of this pair consists of a remarkably flat band at −4 eV for each spin direction.

B. Magnetic tendency

The FM state is favored energetically over the nonmagnetic state by 0.37 eV/Co, similar to the value given by Matsuno *et al.*[14] The spin magnetic moments are 1.95 total, 1.52 from Co and 0.22 from each PO (in units of the Bohr mag-

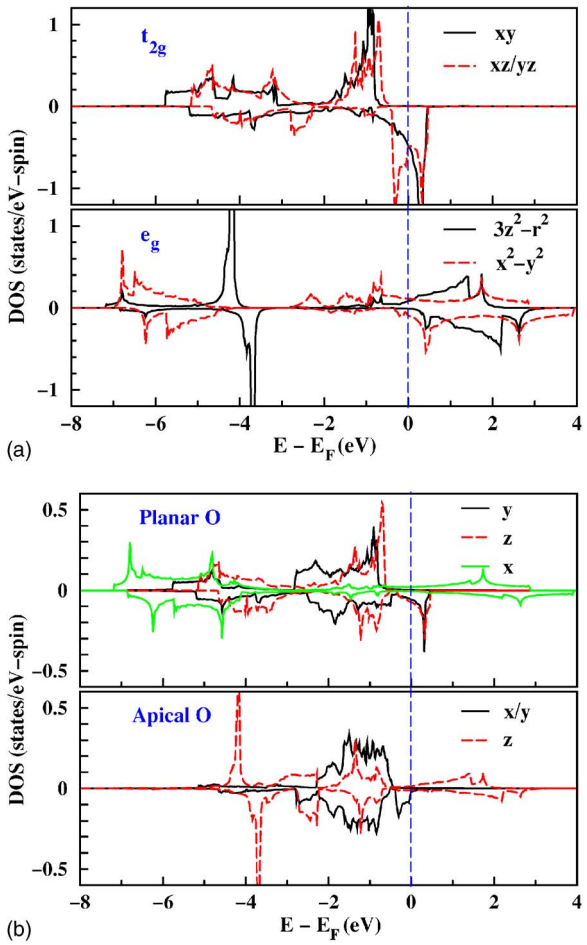

FIG. 4. (Color online) Orbital-projected densities of states for Co $3d$ (upper) and O p states (lower) in LSDA FM calculation. The d_{xz} and d_{yz} states are degenerate. The crystal field splitting of 2 eV between t_{2g} and e_g manifolds is only a little higher than the exchange splitting 1.3 eV. The PO p_x and AO p_z are the σ orbital.

neton). The large magnetic moment for PO, due to strong hybridization with Co $3d$ bands, has been observed previously in Li_2CuO_2[34] and a few other cuprates. The Mullikan decomposition of O charges as well as the band filling of related bands indicates that AO is consistent with its formal designation O^{2-}, whereas PO contributes considerably to the conduction bands and cannot be considered fully ionic. According to the Co $3d$ orbital occupancies given in Table I, however, every $3d$ orbital contributes to the magnetic moment due to itineracy. The variation from average contribution occurs in two states: d_{xy} has 40% larger, and $d_{3z^2-r^2}$ orbital 40% smaller, contributions than the average contribution to the moment. The strong itinerant character (all $3d$ orbitals are neither fully occupied nor fully unoccupied) explains why no Jahn-Teller distortion is observed in Sr_2CoO_4.

The fixed spin moment method[31] is applied in a following subsection to probe the magnetic behavior. In the LSDA fixed spin moment calculations (see below) the low moment region is given by $E(M)-E(0)\approx-\alpha M^2+\beta M^4$ with constants $\alpha=133$ meV/μ_B^2, $\beta=16$ meV/μ_B^4. The Stoner-enhanced susceptibility is given by

$$\chi=\frac{\chi_0}{1-N(0)I}, \tag{3}$$

where the bare susceptibility $\chi_0=2\ \mu_B^2N(0)$ and $N(0)$ is the single-spin density of states at the Fermi level. Also in the low-M limit one obtains formally $\alpha=(1/2)\chi^{-1}$, giving the Stoner interaction $I=1.17(\pm0.05)$ eV. With this value $IN(0)\approx1.7$, giving a very strong Stoner instability of the nonmagnetic phase that is numerically similar to that of nonmagnetic Fe.

C. Fermiology

The LSDA FM Fermi surfaces (FS) pictured in Fig. 5 consist of two sheets from the majority states and four minority sheets, with very simple geometry and strong two-dimensionality. Except for one sheet that has an ellipsoidal shape (majority $d_{3z^2-r^2}$ character), the FSs have the shape of rectangular cylinders with rounded corners. The X-centered sheets contain holes, whereas the Γ-centered surfaces contain electrons. The FS arising from majority $d_{x^2-y^2}$ [Fig. 5(a)] has a clear nesting feature, as does the minority hole sheet in Fig. 5(d). The spanning vectors may lead to spin-density-wave and/or charge-density-wave instabilities. Intrasurface scattering may also show some nesting features. For the most part Fermi velocities v_F are in the range of a few 10^7 cm/s as usual in a metal, but order of magnitude lower velocities occur along the Γ_3 to Z line at E_F.

D. Magnetocrystalline anisotropy

We included spin-orbit coupling by using the fully relativistic FPLO method[30] to allow us to study the strong mag-

TABLE I. Co $3d$ orbital (Mullikan) occupancy in LSDA, where $M=1.95\ \mu_B$. The difference of occupancies between both spin channels is directly related with contribution of each orbital to spin magnetic moment, which can be seen to be spread over all five $3d$ orbitals.

	t_{2g}			e_g	
	E_g		B_{2g}	A_g	B_{1g}
	xz	yz	xy	$3z^2-r^2$	x^2-y^2
Majority	1.00	1.00	1.00	0.56	0.67
Minority	0.68	0.68	0.54	0.36	0.32
Difference	0.32	0.32	0.46	0.20	0.35

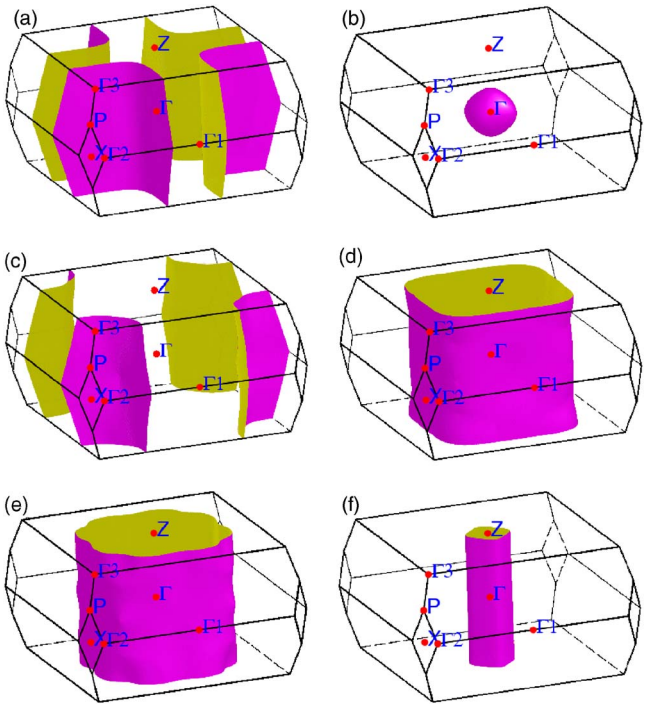

FIG. 5. (Color online) LSDA FM Fermi surfaces, for $M=1.95\ \mu_B$. Surfaces (a) and (b) are from the majority states, surfaces (c)–(f) from the minority bands. While (a) and (c) contain holes, the others enclose electrons. Each surface has mainly (a) $d_{x^2-y^2}$ (0.5 holes), (b) $d_{3z^2-r^2}$ (0.01 electrons), (c) d_{xz} (0.2 holes), (d) d_{xy} (0.4 electrons), (e) d_{yz} (0.4 electrons), and (f) $d_{x^2-y^2}$ (0.02 electrons) characters. The number in parentheses says carrier number containing each Fermi surface per Co.

netic anisotropy reported by Matsuno *et al.*[14] The total energies along ⟨100⟩ and ⟨001⟩ directions were calculated to determine the magnetocrystalline anisotropy energy (MAE). The energy difference $E_{\langle 100\rangle}-E_{\langle 001\rangle}=0.57$ meV/Co is consistent with experimentally observed ⟨001⟩ easy c axis. The relativistic calculations give an orbital magnetic moment of 0.08 μ_B for Co, and negligible values for oxygen ions. The spin and orbital magnetic moments depend on the spin direction, differing by ~5%.

The experimental MAE can be estimated from field dependent magnetization along the two directions.[14] The data show half-saturation at 7 T along the ⟨100⟩ direction. Considering the saturated magnetization to be $M_s=1.8\ \mu_B$/Co, the MAE from M_sB is 1.5 meV/Co, a value three times larger than our calculated result. Such underestimation in LSDA is common for Co compounds. The reason is still unsettled, but candidate explanations are the poor treatment of orbital polarization[35] or for Hubbard-like correlation[36] in the standard LSDA.

Rotating the spin direction induces a change of band structure, as shown in Fig. 6. While the band structure for the moment along ⟨100⟩ direction is essentially that of LSDA, there are additional splittings at several points for the moment oriented along the easy axis. The most visible splitting occurs in Co t_{2g} manifold, where the spin-orbit splitting spans E_F at the Z point. Applying SOC with spin directed along the easy axis, the bands split into primarily

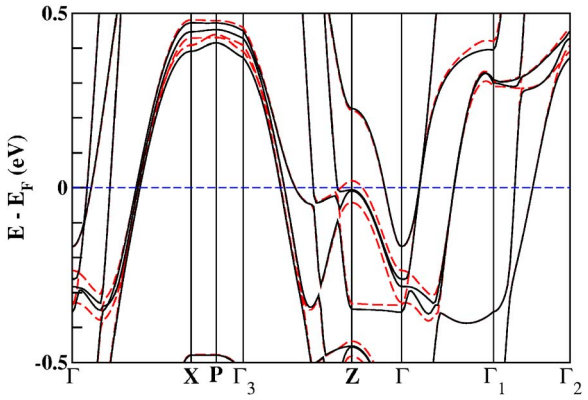

FIG. 6. (Color online) LSDA FM band structures from spin-orbit coupling calculation with the quantization axis along ⟨100⟩ (solid) and ⟨001⟩ (dashed) directions. Note the ⟨001⟩ direction is the easy axis. The dashed horizontal line denotes the Fermi energy.

$d_{j=5/2,m_j=-3/2}$ character in the upper band, and $d_{j=3/2,m_j=1/2}$ in the lower band. The splittings are 60 and 90 meV at the Z and Γ point, respectively.

IV. INCLUSION OF CORRELATION EFFECT

A. Metal to half metal transition

Since the appropriate value of U in this and other cobaltate systems is unclear, we have studied the ground state as U is increased. The moment initially increases slightly in FLL, while it decreases slowly to 1.5 μ_B at $U=2.5$ eV in AMF, as shown in Fig. 7. From their separate states just below and at the critical value $U_c=2.5$ eV, beyond this critical value the moment drops sharply to 1 μ_B in both schemes, and then both schemes produce very similar results in the entire re-

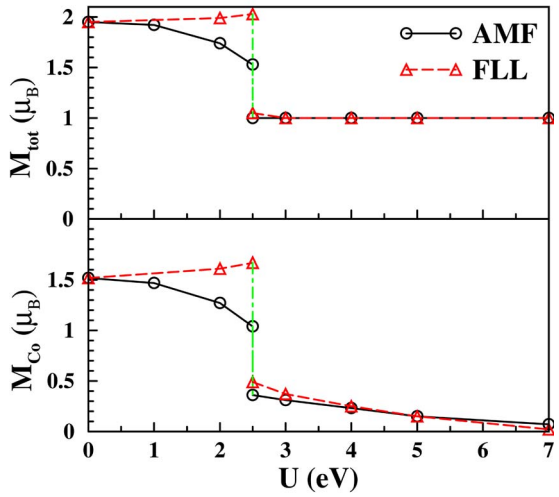

FIG. 7. (Color online) Effect of the on-site Coulomb repulsion U on total and Co local magnetic moments in both LDA+U schemes. At $U_c=2.5$ eV, a metal to half metal transition occurs. The first-order transition is obtained nearly at the same U in both schemes. (In fact, the transition occurs a little higher than U_c in FLL, but the difference is only a few tenths of an electron volt.)

TABLE II. Co 3*d* orbital occupancy in half metallic state, having $M=1\ \mu_B$, at $U=2.5$ eV. Compared to LSDA result shown in Table I, there are two remarkable changes in the e_g state: nearly vanishing contribution of $d_{3z^2-r^2}$ and negative contribution of $d_{x^2-y^2}$ (for details, see text). It seems to be close to LS state, but the $d_{x^2-y^2}$ minority has considerable occupancy due to strong hybridization (itinerary) which makes it impossible to be called strictly as LS state. The total occupation is 6.79.

	t_{2g}			e_g	
	E_g		B_{2g}	A_g	B_{1g}
	xz	yz	xy	$3z^2-r^2$	x^2-y^2
Majority	1.00	1.00	1.01	0.35	0.25
Minority	0.81	0.81	0.44	0.44	0.68
Difference	0.19	0.19	0.57	−0.09	−0.43

gion above U_c. Note particularly that this transition starts from distinct states, but occurs at the same value U_c to the same final state. Both high-moment and low-moment states can be stabilized in the calculations at U_c. Unlike studies in the Na_xCoO_2 system, no discernible hysteretic region could be found at this first-order transition. This magnetic collapse accompanies a metal to half metal transition, presumably because there is a particular stability of this half metallic (HM) FM state since both LDA+U schemes transition to it. The HM state, with a magnetic moment 1 μ_B, has been observed also by Wang *et al.*[16,17] As U increases, the Co local magnetic moment decreases to vanishingly small value by $U\sim 6-7$ eV. The state remains a HM FM, the moment has been pushed onto the PO ions. Since the moment on Co has vanished, it is not surprising that the two LDA+U schemes give the same result.

The microscopic mechanism behind the magnetic collapse induced by the on-site Coulomb repulsion U can be unraveled from a study of the charge decompositions in Tables I and II, and comparison of band structures. We can compare and contrast the two viewpoints. First we point out that, although the Mullikan charges given in these tables are somewhat basis set dependent so their specific magnitude should not be given undue significance, differences—whether between orbitals or between spin-projections—are more physical. Then, while these orbital occupations provide one characterization, we have also provided in Figs. 2 and 8 by the fat-bands technique, the bands that one identifies with $d_{x^2-y^2}$ and $d_{3z^2-r^2}$ character. Using both viewpoints provides a more robust interpretation of behavior than either separately.

From Tables I and II one can determine that increasing U does not change the total 3*d* occupation, but introduces rearrangements in the 3*d* charge and moment. From the bands, the main difference (between FM LSDA and HM FM LDA+U) is that the dispersive majority $d_{x^2-y^2}$ band has become fully *unoccupied*, leaving the small gap that results in half metallicity. Returning to the charges and moments, what stands out is that the moment on the $d_{x^2-y^2}$ orbital has flipped, from +0.35 μ_B to −0.43 μ_B. The $d_{3z^2-r^2}$ moment has undergone a smaller change in the same manner: 0.20 to −0.09 μ_B. Thus the net moment on the Co ion, which is $\sim$0.5 μ_B, is the result of $\sim$+1 μ_B in the t_{2g} orbitals (primarily d_{xy}) and $\sim$−0.5 μ_B in the e_g orbitals. This type of cancellation, in more striking form, has been seen previously in LDA+U results for $LaNiO_2$,[37] which has an unusually *low* formal oxidation state for a nickelate.

B. Fixed spin moment calculation at U_c

The results of the previous section show that two magnetic states coexist at U_c in LDA+U, whether one uses the AMF or FLL functional. Such a coexistence has been already observed in LDA+U calculations for the sodium cobaltates,

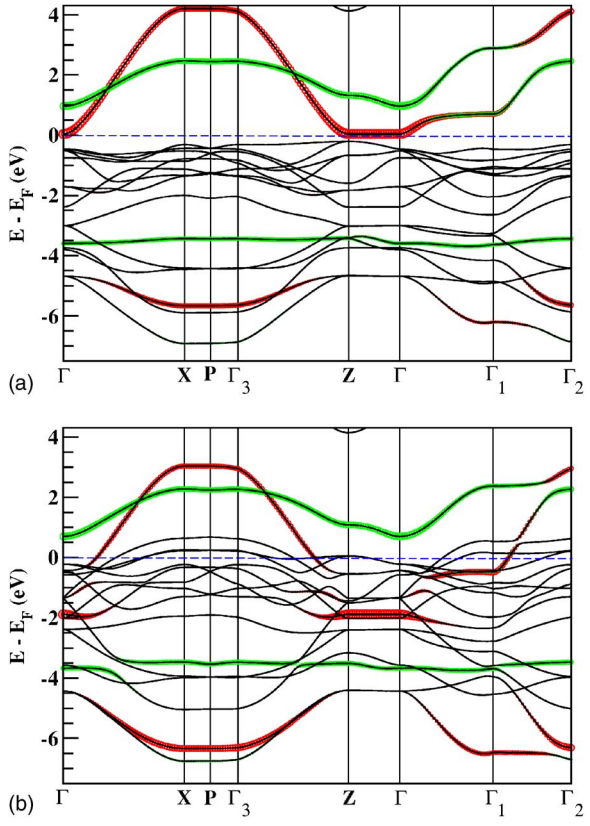

FIG. 8. (Color online) LDA+U FM majority (upper) and minority (lower) band structures at $U_c=2.5$ eV in the half metallic state with $M=1\ \mu_B$. The majority state shows a gap of 0.25 eV. The thickened (and colored) lines emphasize Co $d_{3z^2-r^2}$ (green or light) and $d_{x^2-y^2}$ (red or black) characters. The dashed horizontal line denotes the Fermi energy.

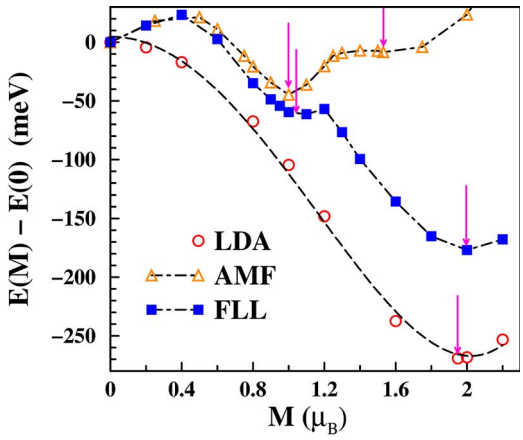

FIG. 9. (Color online) Fixed spin moment calculations in LSDA and both LDA+U schemes at U_c=2.5 eV. The arrows pinpoint (meta)stable states. The dashed line for LSDA FSM indicates fitting line with $E(M)-E(0)=\varepsilon_0-\alpha M^2+\beta M^4$, where ε_0=5 meV, α=133 meV/μ_B^2, and β=16 meV/μ_B^4.

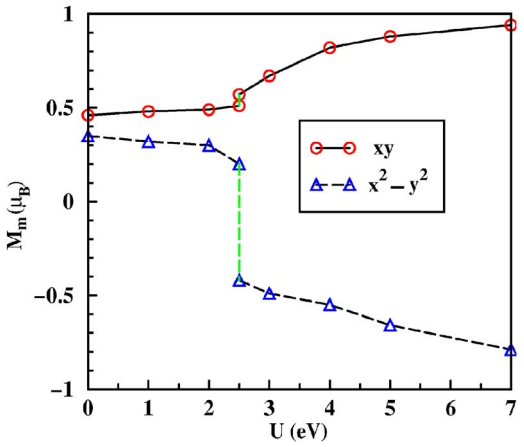

FIG. 10. (Color online) Effect of strength of U on the orbital-projected Co magnetic moment M_m, defined by difference between majority and minority occupancies, of Co $d_{x^2-y^2}$ and d_{xy} states in AMF scheme. (Results for the FLL scheme are similar.) In the large U limit an on-site "singlet" type cancellation of moments occurs in this $m=\pm 2$ channel (see Fig. 7 and text).

where the change at U_c corresponds to a charge disproportionation transition.[38] Here the change is simply in the state of the (single) Co ion; there is no experimental indication of disproportionation here. Here we analyze the FSM results at U_c for LSDA, AMF, and FLL.

The energy versus total magnetic moment behavior, displayed in Fig. 9, shows very interesting differences as well as similarities. Perhaps most interesting is that positions of local minima occur at (or near) integer values M=0, 1, and 2 μ_B, as if there might be underlying states with $S_z=0,\frac{1}{2}$, or 1 pervading the behavior. The results of previous sections, however, established that there is strong $d-p$ hybridization, which renders integral moments no more favored than other values. The LSDA curve shows simple behavior: a Stoner instability at M=0 and a single minimum near (but not precisely at) M=2. The LDA+U results show more interesting variation.

For both AMF and FLL, the paramagnetic state is metastable, with energy rising up to a moment $M\approx 0.5$, and then decreasing very similarly to the minimum at M=1. Beyond that point, AMF levels off to a broad flat region M=1.3–1.8 beyond which it increases with M. FLL however switches over to a separate phase, with its minimum at M=2. The $E(M)$ curve for FLL seems to consist of two separate parabolas (different phases) with minima very near M=1 and M=2. The M=1 result is integral because a half metallic phase is encountered (see Fig. 8) and not due to an S=1/2 configuration of the Co ion. Both majority $d_{x^2-y^2}$ and $d_{3z^2-r^2}$ become completely unoccupied, leaving a small gap to the t_{2g} bands.

We must point out that for both AMF and FLL schemes, the minimum at M=0 μ_B does not correspond to a nonmagnetic state. There is a moment on Co with magnitude 0.14 μ_B that is canceled by magnetization on the PO ion. The driving force for favoring this low, canceling moment phase over a nonmagnetic state is not clear. Possibly an antiferromagnetic result, requiring a doubled unit cell, would be a lower energy M=0 solution.

C. Strong interaction regime

In Sr_2CoO_4 correlation effects should not be very strong it seems, since LSDA already gives a FM state that seems consistent with one of the experimental reports. However, in a strongly correlated regime, but not beyond realistic range of U, there is another interesting feature. Figure 10 shows the U-dependent orbital-projected local magnetic moment M_m, defined by the difference between majority and minority occupancies, of Co $d_{x^2-y^2}$ and d_{xy} states. Upon increasing U, the d_{xy} minority state loses electrons, while the $d_{x^2-y^2}$ minority state gains electrons. Beyond $U=U_c$=2.5 eV, d_{xy} and $d_{x^2-y^2}$ have large positive and negative local magnetic moments respectively, leading to an on-site singlet-type cancellation within this $|m|$=2 channel. This type of cancellation, but within the e_g manifold, has been seen already in our previous results for $LaNiO_2$.[37] In contrast with $LaNiO_2$, which shows the cancellation in the total magnetic moment and $Ni^{1+}\rightarrow Ni^{2+}$ conversion, the moment of the system remains unchanged because of large magnetic moments on planar oxygen ions.

V. SUMMARY

Synthesis of the high formal oxidation state compound Sr_2CoO_4, bulk materials by high-pressure high-temperature techniques and films by pulsed laser deposition (PLD), have led to a high Curie temperature metallic ferromagnet that introduces new transition metal oxide physics and may be useful in spin electronics devices. We have provided an in-depth study of the electronic and magnetic structure of this compound, looking specifically into the combined effects of correlation on the 3d orbitals and strong hybridization with O 2p states.

Within LSDA Sr_2CoO_4 is metallic with a ferromagnetic moment near 2 μ_B, close to the saturation magnetization reported for the PLD films. Application of the two commonly used LDA+U functionals reveals several surprises. As U is increased from zero, the two functionals produce changes

in the moment of opposite sign up to the critical value $U_c = 2.5$ eV. Beyond half metallic ferromagnetic phase with moment 1 μ_B. Within this phase, increasing the value of U has the effect of pushing the moment completely off the Co and onto the planar O ions by $U \sim 6-7$ eV, while the total moment remains fixed at 1 μ_B.

With U fixed at $U_c = 2.5$ eV, fixed spin moment calculations were carried out for both LDA+U functionals, and compared to the corresponding LSDA result. Both LDA+U schemes behaved similarly out to a minimum at 1 μ_B (the half metallic state). Beyond this, the two functionals departed in their behavior, with the FLL scheme jumping to a new state with minimum very near 2 μ_B, not half metallic and much the same as the LSDA minimum (1.95 μ_B). In the stronger-interacting regime $U \geqslant 3$ eV (which may not be appropriate for Sr_2CoO_4), the correlation described by the LDA+U approach leads to oppositely directed moments on the $d_{x^2-y^2}$ and d_{xy} orbitals, reflecting the strong difference in hybridization of these two orbitals.

ACKNOWLEDGMENTS

We acknowledge illuminating conversations with M. Richter for magnetic anisotropy energy and K. Koepernik for technical assistance. This work was supported by DOE Grant No. DE-FG03-01ER45876 and DOE's Computational Materials Science Network. W.E.P. acknowledges the stimulating influence of DOE's Stockpile Stewardship Academic Alliance Program.

[1] K. Takada, H. Sakurai, E. Takayama-Muromachi, F. Izumi, R. A. Dilanian, and T. Sasaki, Nature (London) **422**, 53 (2003).
[2] M. L. Foo, Y. Wang, S. Watauchi, H. W. Zandbergen, T. He, R. J. Cava, and N. P. Ong, Phys. Rev. Lett. **92**, 247001 (2004).
[3] G. C. Amatucci, J. M. Tarascon, and L. C. Klein, J. Electrochem. Soc. **143**, 1114 (1996); J. M. Tarascon, G. Vaughan, Y. Chabre, L. Seguin, M. Anne, P. Strobel, and G. Amatucci, J. Solid State Chem. **147**, 410 (1999).
[4] A. Van der Ven, M. K. Aydinol, G. Ceder, G. Kresse, and J. Hafner, Phys. Rev. B **58**, 2975 (1998).
[5] T. Matsurra, J. Tabuchi, J. Mizusaki, S. Yamauchi, and K. Fueki, J. Phys. Chem. Solids **49**, 1403 (1988).
[6] Y. Furukawa, S. Wada, and Y. Yamada, J. Phys. Soc. Jpn. **62**, 1127 (1993).
[7] Y. Moritomo, K. Higashi, K. Matsuda, and A. Nakamura, Phys. Rev. B **55**, R14725 (1997).
[8] J. Wang, W. Zhang, and D. Y. Xing, Phys. Rev. B **62**, 14140 (2000).
[9] M. Sanchez-Andujar, B. Rivas-Murias, D. Rinaldi, R. Caciuffo, J. Mira, R. Rivas, and M. A. Senaris-Rodriguez, J. Magn. Magn. Mater. **272-276**, 855 (2004).
[10] G. Demazeau, P. Courbin, G. L. Flem, M. Pouchard, P. Hagenmuller, J. L. Soubeyroux, I. G. Main, and G. A. Robins, Nouv. J. Chim. **3**, 171 (1979).
[11] Y. Y. Liu, X. M. Chen, and X. Q. Liu, Solid State Commun. **136**, 576 (2005).
[12] C. N. R. Rao, P. Ganguly, K. K. Singh, and R. A. Mohan Ram, J. Solid State Chem. **72**, 14 (1988).
[13] K. Yamada, M. Matsuda, Y. Endoh, B. Keimer, R. J. Birgeneau, S. Onodera, J. Mizusaki, T. Matsuura, and G. Shirane, Phys. Rev. B **39**, 2336 (1989).
[14] J. Matsuno, Y. Okimoto, Z. Fang, X. Z. Yu, Y. Matsui, N. Nagaosa, M. Kawasaki, and Y. Tokura, Phys. Rev. Lett. **93**, 167202 (2004).
[15] J. Matsuno, Y. Okimoto, Z. Fang, X. Z. Yu, Y. Matsui, N. Nagaosa, H. Kumigashira, M. Oshina, M. Kawasaki, and Y. Tokura, Thin Solid Films **486**, 113 (2005).
[16] X. L. Wang and E. Takayama-Muromachi, Phys. Rev. B **72**, 064401 (2005).
[17] X. L. Wang, H. Sakurai, and E. Takayama-Muromachi, J. Appl. Phys. **97**, 10M519 (2005).
[18] T. Tekeda, T. Watanabe, S. Komura, and H. Fujii, J. Phys. Soc. Jpn. **56**, 731 (1987).
[19] S. Mathi Jaya, R. Jagadish, R. S. Rao, and R. Asokamani, Phys. Rev. B **43**, 13274 (1991).
[20] R. H. Potze, G. A. Sawatzky, and M. Abbate, Phys. Rev. B **51**, 11501 (1995).
[21] M. A. Korotin, S. Yu Ezhov, I. V. Solovyev, V. I. Anisimov, D. I. Khomskii, and G. A. Sawatzky, Phys. Rev. B **54**, 5309 (1996).
[22] H. Takahashi, F. Munakata, and M. Yamanaka, Phys. Rev. B **57**, 15211 (1998).
[23] I. A. Nekrasov, S. V. Streltsov, M. A. Korotin, and V. I. Anisimov, Phys. Rev. B **68**, 235113 (2003).
[24] G. Maris, Y. Ren, V. Volotchaev, C. Zobel, T. Lorenz, and T. T. M. Palstra, Phys. Rev. B **67**, 224423 (2003).
[25] D. Phelan, Despina Louca, S. Rosenkranz, S.-H. Lee, Y. Qiu, P. J. Chupas, R. Osborn, H. Zheng, J. F. Mitchell, J. R. D. Copley, J. L. Sarrao, and Y. Moritomo, Phys. Rev. Lett. **96**, 027201 (2006).
[26] K. Koepernik and H. Eschrig, Phys. Rev. B **59**, 1743 (1999).
[27] V. I. Anisimov, I. V. Solovyev, M. A. Korotin, M. T. Czyzyk, and G. A. Sawatzky, Phys. Rev. B **48**, 16929 (1993).
[28] M. T. Czyzyk and G. A. Sawatzky, Phys. Rev. B **49**, 14211 (1994).
[29] S. L. Dudarev, G. A. Botton, S. Y. Savrasov, C. J. Humphreys, and A. P. Sutton, Phys. Rev. B **57**, 1505 (1998).
[30] H. Eschrig, M. Richter, and I. Opahle, in *Relativistic Electronic Structure Theory –Part II: Applications*, edited by P. Schwerdtfeger (Elsevier, Amsterdam, 2004), pp. 723–776.
[31] K. Schwarz and P. Mohn, J. Phys. F: Met. Phys. **14**, L129 (1984).
[32] L. F. Mattheiss, Phys. Rev. Lett. **58**, 1028 (1987).
[33] For review, see W. E. Pickett, Rev. Mod. Phys. **61**, 433 (1989).
[34] R. Weht and W. E. Pickett, Phys. Rev. Lett. **81**, 2502 (1998).
[35] H. Eschrig, M. Sargolzaei, K. Koepernik, and M. Richter, Europhys. Lett. **72**, 611 (2005).
[36] D. Mertz, R. Hayn, I. Opahle, and H. Rosner, Phys. Rev. B **72**, 085133 (2005).
[37] K.-W. Lee and W. E. Pickett, Phys. Rev. B **70**, 165109 (2004).
[38] K.-W. Lee, J. Kuneš, P. Novak, and W. E. Pickett, Phys. Rev. Lett. **94**, 026403 (2005).